Marine and Petroleum Geology 130 (2021) 105129

Contents lists available at ScienceDirect

Marine and Petroleum Geology

journal homepage: www.elsevier.com/locate/marpetgeo

Research paper

Kinetics and fate of organosulphur compounds during the metagenesis stage of thermal maturation: Hydrous pyrolysis investigations on dibenzothiophene

Xiao Jin [a,b,c], Jia Wu [a,b,*], Peng Fang [a,b], Zhihuan Zhang [a,b], Meijun Li [a,b], Ningning Zhong [a,b]

[a] State Key Laboratory of Petroleum Resources and Prospecting, China University of Petroleum (Beijing), Beijing, 102249, China
[b] College of Geosciences, China University of Petroleum (Beijing), Beijing, 102249, China
[c] Department of Geoscience, University of Calgary, 2500 University Drive NW, Calgary, AB, T2N 1N4, Canada

ARTICLE INFO

Keywords:
Dibenzothiophene
Organosulphur compounds
Thermal maturation
Organic-derived H_2S
S cycle
Ultra-deep stratum

ABSTRACT

Organosulphur compounds (OSCs) play important roles in the formation, preservation, and thermal degradation of sedimentary organic matter associated with petroleum generation. However, with the ongoing develop of hydrocarbon prospecting in ultra-deep reservoirs, the thermal maturation and geochemical behaviours of OSCs in deep sedimentary basins during the metagenesis stage of thermal maturation has not been well understood. In this study, we modelled the thermal maturation of OSCs by a combination of gold-tube hydrous pyrolysis studies and quantum mechanics calculations based on density functional theory (DFT) to investigate the reaction pathways and kinetic properties. Dibenzothiophene (DBT) was selected as an over-mature model molecule due to its high degree of aromaticity and lack of side chains. The energy barrier of aryl-aryl bonding is estimated to be approximately 60 kcal/mol. Dehydrogenation of OSCs through aryl-aryl bonding mainly occurs in the Easy%R_o range of 2.3%–3.8%. We modeled the contribution of OSCs to organic-derived H_2S at advanced maturity based on numerical simulations in MATLAB. The contribution of OSCs to H_2S can be quantitatively predicted based on specific thermal histories and the kinetics of H release from biaryl formation. Taking the Sinian reservoirs in the central uplift of the Sichuan Basin as an example, the yield of organic-derived H_2S contributed from S-rich solid bitumen (S/C atomic ratio ~0.06) was estimated to be approximately 1.58 mg/g. These results suggested that OSCs participated as carriers of organic S from the surface to deep strata. Desulphurisation of OSCs together with thermochemical sulphate reduction, could contribute to the subsurface accumulation of H_2S, to the detriment of. the quality of hydrocarbon reservoirs and the durability of the drill.

1. Introduction

Organosulphur compounds (OSCs) are formed by the incorporation of reduced inorganic sulphur species into functionalised lipids through microbial sulphate reduction (MSR), thermochemical sulphate reduction (TSR), or geochemical transformations of polysulphide anions (Amrani, 2014; Amrani and Aizenshtat, 2004; Ellis et al., 2017; Machel, 2006; Werne et al., 2003). OSCs play important roles in the formation, preservation, and thermal degradation of sedimentary organic matter associated with petroleum generation (Amrani, 2014; Ho et al., 1974; Lewan et al., 2006). Furthermore, OSCs have been increasingly used as geochemical tracers for studying source rock-oil or oil-oil correlation (Cai et al., 2009; Li et al., 2013), indicating depositional environments (Hughes et al., 1995; Radke et al., 2000), the maturity of organic matter (Chakhmakhchev et al., 1997; Ho et al., 1974; Radke, 1988; Santamaría-Orozco et al., 1998), oil charging pathways in reservoirs (Fang et al., 2016; Li et al., 2014), as well as TSR (Amrani et al., 2012; Ellis et al., 2017). The thermal maturation of OSCs generally results in a net loss of S (Amrani et al., 2005; P Koopmans et al., 1998), induced by temperature elevation during the progressive burial of organic matter in sedimentary basins (Amrani, 2014). For example, the release of H_2S has been observed during the thermal treatment of both synthetic polysulphide cross-linked macromolecules and S-rich kerogens (Birdwell et al., 2018; Krein and Aizenshtat, 1995; Orr, 1986). S-bearing radicals can destabilise hydrocarbons and promote kerogen degradation during the diagenesis stage (Lewan, 1997). However, Kelemen et al. (2010)

* Corresponding author. State Key Laboratory of Petroleum Resources and Prospecting, China University of Petroleum (Beijing), Beijing, 102249, China.
E-mail addresses: jinx622109@foxmail.com (X. Jin), jia.wu@cup.edu.cn (J. Wu), zhangzh3996@vip.163.com (Z. Zhang), meijunli@cup.edu.cn (M. Li), nnzhong@126.com (N. Zhong).

https://doi.org/10.1016/j.marpetgeo.2021.105129
Received 2 May 2020; Received in revised form 18 March 2021; Accepted 8 May 2021
Available online 18 May 2021

reported that the S/C ratio remains relatively constant in high-maturity pyrobitumens, which they attributed to the gradual conversion of aliphatic sulphides to aryl sulphides such as thiophene and derivatives.

Ultra-deep reservoirs (>6500 m) have attracted considerable attention in recent years due to the rapid advances in prospecting, drilling, and extraction techniques (Guan et al., 2019; Zhu et al., 2012). Significant accumulation of hydrocarbons has been observed in Precambrian strata (Ara carbonate stringer play in South Oman Salt Basin and carbonate sediments of Dengying Formation in Sichuan Basin; Grosjean et al., 2009; Liu et al., 2018), accompanied by solid bitumen precipitates (Li et al., 2020; Schoenherr et al., 2007; Yang et al., 2018). Additionally, abundant H_2S and S-rich solid bitumens have been discovered in various ancient and ultra-deep strata (Song et al., 2017; Wacey et al., 2015; Zhang et al., 2019; Zhu et al., 2019a). The prevailing hypothesis has attributed this accumulation of H_2S to the TSR of petroleum in the presence of inorganic sulphate minerals such as gypsum. However, the presence of natural gas reserves enriched in H_2S and OSCs, but without gypsum-bearing strata, has also been reported (Zhu et al., 2018). Laboratory studies conducted at higher temperature and pressure are required to understand the contribution of OSCs to organic-derived H_2S at much greater depths.

Here we conducted gold-tube hydrous pyrolysis experiments to investigate the kinetic characteristics of OSCs at advanced maturity. Dibenzothiophene (DBT) was selected as a model organosulphur compound because it is relatively stable (Dartiguelongue et al., 2006), highly aromatised, widely distributed in crude oils and solid bitumens (Asif et al., 2009; Greenwood et al., 2018; McCollom et al., 2015), and similar in S/C atomic ratio (0.08) to S-rich solid bitumens (0.06; Zhang et al., 2019). Furthermore, we probed the mechanistic pathways for biaryl formation from DBT using the quantum mechanics density functional theory (DFT), and estimated the contribution of OSCs to H_2S production during the metagenesis stage of thermal maturation through MATLAB simulations.

2. Methods

2.1. Samples

Dibenzothiophene was purchased from Alfa Aesar and its purity was assessed by gas chromatography-mass spectrometry. Main impurities included biphenyl (<0.3 wt%), dibenzofuran (<0.1 wt%), and fluorene (<0.1 wt%). Deionised water was treated in a Direct-Pure UP Ultrapure & RO Lab Water System and Tank Sanitisation Module purchased from Rephile Bioscience. The biphenyl standard was purchased from Acros Organics. The benzothiophene standard was purchased from Adamas-beta. Methyl-dibenzothiophene, phenyl-dibenzothiophene, dibenzofuran, and fluorene standards were purchased from Alfa Aesar. The dimethyl-dibenzothiophene standard was purchased from Tokyo Chemical Industry CO.

2.2. Experiments

2.2.1. Gold-tube pyrolysis

All pyrolysis experiments were conducted using a gold tube thermal simulation instrument (ST-120-II) at the Thermal Simulating Lab for Generation and Expulsion of Petroleum, affiliated to the State Key Laboratory of Petroleum Resources and Prospecting. Briefly, each gold tube (30 mm in length, 5 mm o.d., and 0.25 mm thick) was sealed on one end by welding, and flushed with argon using a LAMPERT PUK U4 (Gesswein CO) argon arc welder coupled to a USM welding microscope. After the sample was loaded, the open end of the tube was flattened to reduce the volume of empty space inside the tube, and then welded in an argon atmosphere. The structural integrity of the capsule was examined by verifying whether there was any weight loss after autoclaving. In each experiment, the temperature of the cell was programmatically increased to the target temperature within 1 h and the pressure was maintained at 50 MPa. Time recording was initiated as soon as the temperature inside the cell reached the preset target. Once the experiment ended, the capsule was slowly cooled to <100 °C over a period of approximately 4 h. The duration of the reaction, temperature, and amount of water loaded into the gold cell in each experiment are summarised in Table 1.

2.2.2. Determination of the chemical composition of gas products

The pyrolysis experiments conducted at 500 °C for 360 h produced sufficient gaseous products, which allowed the chemical composition of the gas mixture to be determined. A volume-calibrated auxiliary cylinder was used to release the gas mixture from the gold tube after the end of each experiment. Briefly, after the gold tube was placed in the auxiliary instrument, the latter was vacuumed until the pressure was reduced to less than 100 Pa. The gold tube was then pierced and the resultant increase in the internal pressure of the cylinder was recorded (Zhang et al., 2013). This pressure increase was then used to calculate the total amount of gas products trapped inside the gold tube based on the assumption of ideal gas behaviour ($PV = nRT$; Zhang et al., 2007).

Each gas compound was identified and quantified on a two-channel 7890 Series Gas Chromatograph (GC; Agilent, USA) integrated with an auxiliary oven, which was custom-configured by Wasson-ECE instrumentation (Fort Collins, CO). The instrument was equipped with two capillary and six-packed analytical columns, a flame ionisation detector (FID), and two thermal conductivity detectors (TCD). The carrier gases for FID and TCD were high-purity N_2 and He, respectively. The temperature of the GC oven was programmed as follows: 68 °C for 7 min, from 68 °C to 90 °C at a linear rate of 10 °C/min, 90 °C for 1.5 min, from 90 °C to 175 °C at a linear rate of 15 °C/min, and finally 175 °C for 5 min. The calibration of the chromatograph response was performed with external gas standards, each of which was prepared at a precision of less than ±1 mol% (He et al., 2018).

2.2.3. Analysis of liquid and solid products

Following the completion of each experiment, the gold tube was flash-frozen in liquid nitrogen for 30 s, transferred to a clean vial filled with dichloromethane (DCM), and then swiftly sliced into several pieces. The vial was capped and sonicated three times, each for 5 min. After the resultant mixture was filtered to recycle the gold residuals and DCM-insoluble OSCs, the flow-through was collected, diluted in DCM, and then injected into an HP-5MS fused silica capillary column (i.d. 60 mm × 0.25 mm, with a 0.25 μm coating; Agilent, USA) on an Agilent 6890 Gas Chromatography coupled to an Agilent 5975i Mass Spectrometer. Helium was used as the carrier gas. The temperature of the GC oven was initially set to 80 °C, then increased linearly to 310 °C at a rate of 3 °C/min, and finally maintained at 310 °C for 45 min. The injection temperature was set to 300 °C. The mass spectrometer was operated in full-scan and SIM mode. Electron impact ionisation was employed with the ionisation voltage set to 70 eV (Li et al., 2012; Shi et al., 2014).

A series of standard solutions, each containing a mixture of DBT, biphenyl (BP), 4-methyl-dibenzothiophene (4-MDBT), 4,6-dimenthyl-dibenzothiophene (4,6-DMDBT), 4-phenyl-dibenzothiophene (4-Ph-DBT), dibenzofuran (DBF), fluorene (FL), and benzothiophene (BT) in a specific concentration ratio, were prepared for the identification and quantification of pyrolysis products that were detected by GC-MS. The

Table 1
Experimental conditions for the pyrolysis of dibenzothiophene at 50 MPa.

Temperature (°C)	Time (h)	m(DBT):m(H_2O) (wt %)
400	168, 408	3:10
420	96, 168, 408	3:10
450	96, 168, 408	3:10, anhydrous, 1:10
480	72, 168, 408	3:10
490	72, 168, 336, 408	3:10
500	72, 168, 360	3:10

chemical identity of each volatile OSC was determined by comparing its relative retention time to that of a known standard and searching for its MS spectral patterns in the NIST mass spectral Library. After the GC-MS analysis, the DCM-soluble OSCs were air-dried and weighed.

Dichloromethane-insoluble OSCs are often produced at high *P-T*. After filtering, these insoluble OSCs were also recovered, air-dried, and weighed. The S/C weighed ratios of both DCM-soluble and DCM-insoluble OSCs were measured on a LECO CS-230 analyser (USA).

2.3. Kinetic modelling of the hydrous pyrolysis of DBT

The kinetic of DBT polymerisation was modelled. Based on the studies of Dartiguelongue et al. (2006), DBT pyrolysis in confined anhydrous systems follows first-order kinetics defined by eq. (1) below:

$$k_T = \ln[1 / (1 - XT)] / t \quad (1)$$

where k_T and t denote the rate constant and the duration of the experiment, respectively. X_T represents the fraction of the reaction completed at the end of the experiment at a given temperature (T), and can be obtained from the equation X_T (%) = 100 × (1– residual DBT/initial DBT). The natural log of k_T was subsequently plotted against the reciprocal of T (in degrees Kelvin). The activation energy (E_a) and frequency factor (A) of the reaction were derived from the slope and intercept of the linear plot, respectively:

$$\ln k = \ln A - E_a/RT \quad (2)$$

where R is the ideal gas constant.

It should be emphasised that the experimental system in the current study represents a greatly simplified model for the thermal maturation of OSCs in natural petroleum reservoirs. The formation of BP and BT was kinetically characterised by plotting the yields of both compounds, from which the maximum yield was derived by extrapolating the linear fit curve to the hypothetical point that corresponded to 100% decomposition of DBT. The generated fractions (X_T) of BP and BT in each hydrous pyrolysis experiment were calculated. As shown by eq. (1) and eq. (2), ln (1-X_T) correlates linearly with time at all temperatures, from which the kinetic parameters (E_a and A) for the formation of BP and BT were then determined.

2.4. Computational model of aryl-aryl bonding

The formation of aryl-aryl bonds is a prevalent phenomenon in organic matter undergoing thermal maturation. Biaryls have been vigorously investigated in crude oils and coals of varying degrees of maturity (Rospondek et al., 2008; Walters et al., 2015; Zhu et al., 2019b). Under high *P-T* conditions, DBT can be converted to biaryls via the following two possible pathways:

2DBT → DBT-dimers + H_2 (primary)

DBT + Benzene → Ph-DBT + H_2 (secondary)

The energy barriers of both reactions were calculated by the Gaussian 09 software. The molecular geometry of the reactants (R), products (P), and transition states (TS) were fully optimised using the M06–2X flavour of the density functional theory (Zhao and Truhlar, 2008). The total electron energy (E_0) was determined with the def2-TZVPP basis set, whereas the zero-point energy (ZPE) and Gibbs' free energy at T (δG) were calculated via 6–311++G**. All stationary points were positively identified for local minima (zero imaginary frequencies) and for the transition state (only one imaginary frequency). Vibrational frequencies were also calculated at all stationary points to obtain zero-point energies (ZPE) and the associated thermodynamic parameters. Solvation effects were included using the solvation model based on solute electron density (SMD; Marenich et al., 2009).

The change in the total Gibbs' free energy $\triangle G(T)$ at temperature T was calculated from the equation below:

$$\Delta G(T) = E_0 + ZPE + \delta G + E_{sol}$$

where E_0 is the total electronic energy (the total internal energy at $T = 0$ K), ZPE represents the term for zero-point energy correction, δG represents the change of Gibbs' free energy from 0 K to T, and E_{sol} is the solvation energy. The transition barrier E_a is defined as:

$$E_a = \Delta G(TS) - \Delta G(R)$$

where $\triangle G$(R) and $\triangle G$(TS) are the Gibbs' free energies of the reactant and transition state, respectively. The temperature and pressure were set to 25 °C and 1 atm, respectively.

3. Results

3.1. General pyrolysis products

The gas products released from the hydrous pyrolysis of DBT comprised CH_4, C_2H_6, C_3H_8, CO_2, H_2S, and H_2, but not butane or pentane (Table 2). The residuals were extracted with DCM, and the soluble fraction was analysed by GC-MS. The chemical composition of the DCM extracts was shown to be highly similar to that reported in a previous study by Dartiguelongue et al. (2006), with BP as the most abundant product (Table 3 & Fig. 1). The yield of BP at 490 °C increased linearly with time until reaching a peak value of 14.84 mg/g DBT at 336 h, followed by a steady decline to 11.81 mg/g DBT at 408 h (Table 4 & Fig. 2). Evidently, BP was generated from the fragmentation and the resultant desulphurisation of DBT. Moreover, BT was another molecular fragment of DBT that we detected, which was likely derived from the hydrocracking of one of the two benzene rings in DBT (Dartiguelongue et al., 2006). This was supported by the identification of 4H-DBT, a key intermediate of DBT hydrogenation (Fig. 1). The DCM-soluble fraction also contained compounds that apparently resulted from DBT polymerisation, such as Ph-DBTs and DBT-dimers (DIs). The maximum yield of DIs at 490 °C reached 50.58 mg/g DBT at 336 h, corresponding to a DBT conversion rate of 36.23% (Table 4). In addition, there were a number of alkyl-substituted DBTs, including methyl-dibenzothiophene (MDBT), dimenthyl-dibenzothiophene (DMDBT), and various benzo-bis-benzothiophene isomers (BBBTs).

Interestingly, the GC-MS analysis also detected trace amounts of dibenzofuran (DBF) and fluorene (FL) at 490 °C, which were not observed in the anhydrous pyrolysis experiments. Unfortunately, these compounds were difficult to accurately characterise due to their low abundances (Table 4). To address this problem, we conducted additional pyrolysis experiments at 450 °C for 96 h in both anhydrous and hydrous systems. Thermal decomposition of DBT in the presence of excessive water exhibited a significantly higher level of DBF than under anhydrous conditions (Table A). Conversely, we did not observe any statistically significant difference in the concentration of FL between the two sets of experiments, suggesting that it was likely an impurity.

Next, we determined the S/C mass ratios of all DCM-soluble fractions and DCM-insoluble residues in two experiments: one at 490 °C for 408 h and another at 500 °C for 360 h (Table 4 & Fig. 3). The equivalent level of thermal maturity achieved in each experiment was estimated by calculating Easy%R_o from the reaction temperature and time (Sweeney and Burnham, 1990). The inverse correlation between the S/C ratio and thermal maturity suggested a gradual loss of S, likely in the form of H_2S, from the thermally decomposing DBT. Desulphurisation of DBT

Table 2
Yields of gaseous products (mg/g) in pyrolysis experiments that lasted for 360 h at 500 °C. m(H_2O):m(DBT) = 100:30.

CH_4	C_2H_6	C_3H_8	CO_2	H_2S	H_2
6.21	6.55	0.52	14.18	7.41	1.11

Table 3
Abbreviations and chemical structures of the main products detected by GC-MS.

Compounds	Abbreviations	Chemical structures
Biphenyl	BP	
Benzothiophene	BT	
Tetrahydro-dibenzothiophene	4H-DBT	
Methyl-dibenzothiophene	MDBT	
Dimethyl-dibenzothiophene Ethyldibenzothiophene	DMDBT C_2-DBT	
Phenyl-dibenzothiophene	Ph-DBT	
Benzo-bis-benzothiophene	BBBT	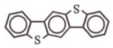
Diphenyl-dibenzothiophene Biphenyl-dibenzothiophene	Ph_2-DBT Biph-DBT	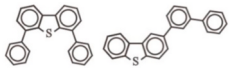
Dimers-dibenzothiophene	DI	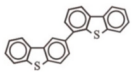
Dibenzofuran	DBF	

occurred when Easy%R_o reached 3.0%, whereas DCM-insoluble OSCs were observed at Easy%R_o above 3.8%. The DCM-insoluble OSCs contained lower levels of S compared with their DCM-soluble counterparts.

3.2. Kinetic parameters for the hydrous pyrolysis of DBT

We plotted the fraction reacted (X_T) in each hydrous pyrolysis experiment, of which the m(H_2O):m(DBT) was 100:30, against time. As expected, ln(1-X_T) correlated linearly with time at all temperatures (Fig. 4a). The mathematical relationship between the apparent rate constant and temperature can be described by eq. (1). As shown in Fig. 4b, our results demonstrated that the hydrous pyrolysis of DBT followed first-order kinetics. Based on these data, the apparent activation energy (E_a) and frequency factor (A) for the thermal decomposition of DBT in hydrous systems were calculated to be 60.68 ± 4.76 kcal/mol and 1.94×10^{11} s^{-1}, respectively.

Furthermore, we investigated the kinetics of BP and BT formation. As elucidated earlier, the yield of BP peaked during the late stage of DBT pyrolysis and then declined sharply (Fig. 2). We extrapolated the linear plot to the hypothetical data point that corresponded to the complete conversion of DBT (Fig. 5a). The result suggested that the maximum hypothetical yield of BP would be 32.67 mg/g DBT. The rate constants (k_T) at different temperatures are shown in Fig. 5b. Following the same method described above, the apparent activation energy and frequency factor for BP formation were calculated to be 53.79 kcal/mol and 1.66×10^9 s^{-1}, respectively (Fig. 5c). On the other hand, the activation energy and frequency factor for BT formation were calculated to be 58.55 kcal/mol and 4.12×10^{10} s^{-1}, respectively (Fig. 6). Importantly, these kinetic parameters can only represent the generation of BP and BT in a closed system without any external H sources.

To further validate our experimental data, we calculated the activation energy for the conversion of DBT to DI and Ph-DBT by quantum mechanical calculations based on the equations below (Table 5, Fig. 7 and Fig. 8):

$$2DBT \rightarrow 2DBT\cdot + 2H\cdot \rightarrow DI + H_2 \quad E_a = 121.51\ kcal/mol$$

$$Benzene + DBT \rightarrow Benzene\cdot + DBT\cdot + 2H\cdot \rightarrow Ph-DBT + H_2 \quad E_a = 117.54\ kcal/mol$$

The above results were then normalised to 1 mol of DBT (note that the stoichiometric ratio of benzene to DBT is 1:1). Therefore, our theoretic calculations indicated that 1 mol of DBT needs to overcome an energy barrier of 60.76 kcal to form 0.5 mol of DI, whereas the activation energy for the coupling of 0.5 mol of benzene and 0.5 mol of DBT (1 mol of reactant molecule) to generate 0.5 mol of Ph-DBT is 58.77 kcal. These data were in excellent agreement with the experimentally obtained values.

4. Discussions

4.1. Interactions of OSCs in DBT closed system

The detection of trace amounts of 4H-DBT and DBF in the products of DBT pyrolysis provided important mechanistic insights. We speculated that 4H-DBT likely resulted from DBT hydrocracking or hydrogenation (Klimova et al., 2013; Lee and Ng, 2006). The thermal cleavage of C–C bonds in 4H-DBT could lead to the formation of benzothiophene and gaseous hydrocarbons. Conversely, the yield of DBF was found to increase with the proportion of water in the experiment system, suggesting that the S in DBT might have been gradually replaced by the O from H_2O (Table A).

Based on these considerations, we hypothesized that the hydrous pyrolysis of DBT begins with its dimerisation and the concomitant generation of H_2, which then reacts with one of the phenyl rings in another DBT molecule to afford 4H-DBT (Fig. 9). The thermal decomposition of 4H-DBT gives rise to BT and various hydrocarbon radicals, the latter of which then adds to DBTs to form alkyl-substituted DBTs such as MDBT or DMDBT. Alternatively, the labile C–S bonds in DBT undergo homolytic cleavage under high *P-T* conditions and react with H_2 to furnish biphenylthiol, which is unstable and immediately fragments into a phenyl radical and a thiol radical. The biphenyl radical subsequently converts to BP by either recombining with a hydrogen radical or reacting with a hydrogen molecule. Meanwhile, BP itself is also prone to homolytic cleavage, which results in the generation of two phenyl radicals. Both BP and phenyl radicals can react with DBT through aromatic addition to generate a wide array of differently substituted phenyl- or biphenyl-DBTs (Ph- or Biph-DBT). In particular, the aromatic addition of a thiol radical to Ph-DBT, followed by S–H bond cleavage and a second aromatic addition reaction, can lead to the formation of benzo-bis-benzothiophene (BBBT; Reckendorf, 2000). It should be emphasised that Ph-DBT, DI, and BBBT have all been detected in oils, coals, and TSR-altered bitumens (Rospondek et al., 2008; Walters et al., 2015). Taken together, these results support to the occurrence of aryl-aryl coupling in subsurface petroleum reservoirs.

In addition, compared to the anhydrous pyrolysis experiments reported by Dartiguelongue et al. (2006), our study showed a similar product profile but a decrease in the conversion rate of DBT. This suggests that water did not alter the main mechanistic pathways of DBT pyrolysis, but rather served as a kinetic inhibitor, likely by shielding DBT molecules from mutual collision. As corroborating evidence, our kinetic investigations indicated that the hydrous pyrolysis of DBT exhibited higher activation energy and lower frequency factor than the same reaction conducted in a water-free system.

4.2. Characterisation of the thermal maturation of high-maturity OSCs

In the current study, the apparent activation energy for the hydrous pyrolysis of DBT was determined to be 60.68 kcal/mol, which is consistent with a previously reported value of 59.00 kcal/mol (Dartiguelongue et al., 2006). The agreement provides evidence that DBT pyrolysis in hydrous and anhydrous geological environments likely shares similar reaction mechanisms. Although it is impractical to experimentally determine the kinetic parameters of each individual coupling or fragmentation reaction, quantum chemistry-based computational methods can provide a close estimate. Theoretical calculations indicated that the activation energies for the conversion of DBT to DBT-dimers (DI) and phenyl-DBT (Ph-DBT) are 60.76 kcal/mol and

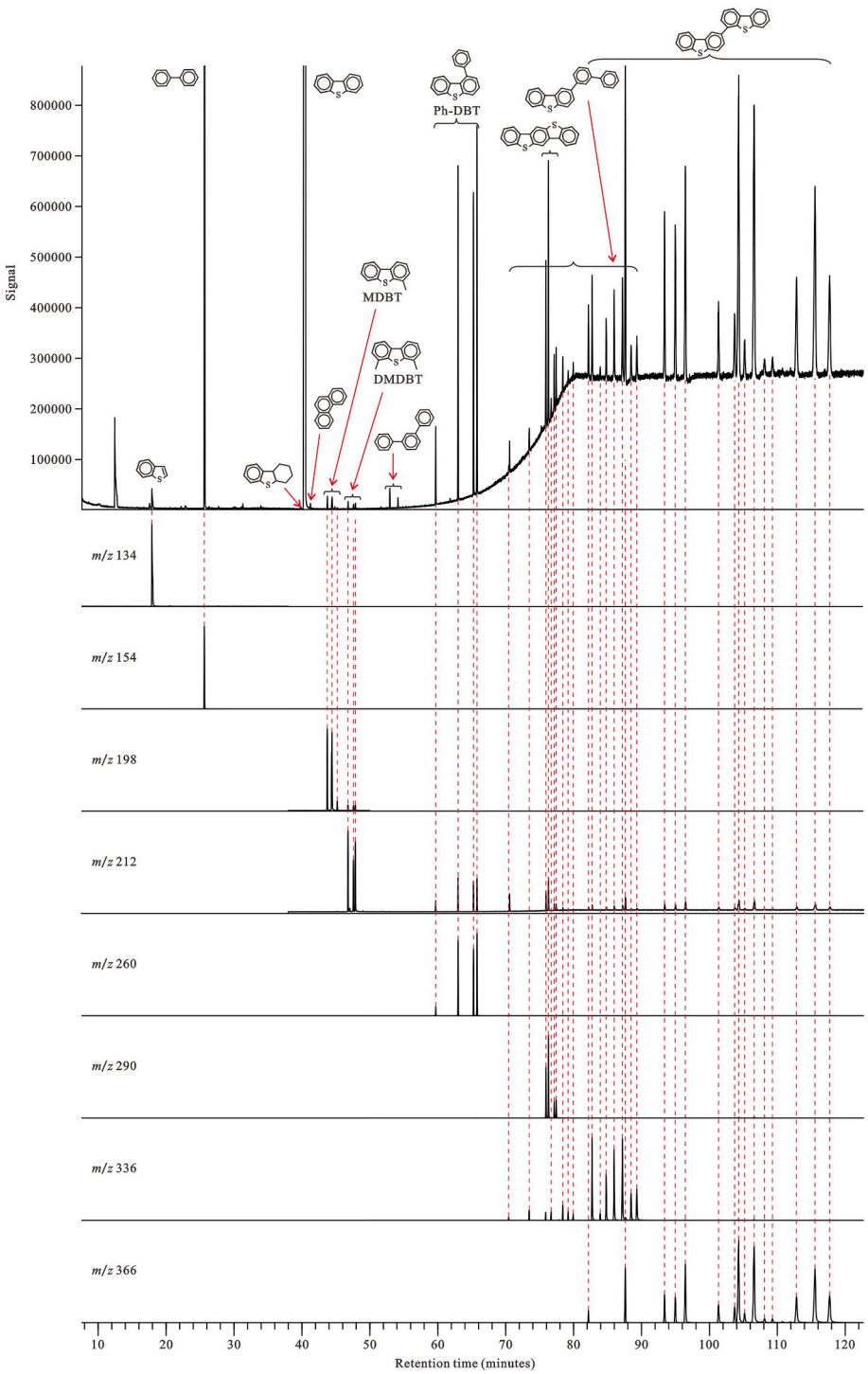

Fig. 1. Total ion chromatograms of products generated from the hydrous pyrolysis of DBT at 490 °C and 336 h. Reconstructing ion chromatograms: m/z 134: Benzothiophene (BT); m/z 154: Biphenyl (BP); m/z 198: Methyl-dibenzothiophene (MDBT); m/z 212: Dimenthyl-dibenzothiophene (DMDBT); m/z 260: Phenyl-dibenzothiophene (Ph-DBT); m/z 290: Benzo-bis-benzothiophene (BBBT); m/z 336: Diphenyl-dibenzothiophene or Biphenyl-dibenzothiophene (Ph_2-DBT or Biph-DBT); and m/z 366: Dimers-dibenzothiophene (DI).

58.77 kcal/mol, respectively, which are in close agreement with the experimentally determined values. Furthermore, the formation of BP and BT required activation energies of 53.79 kcal/mol and 58.55 kcal/mol, respectively. Evidently, the energy barrier for the coupling of DBT to form DI (60.76 kcal/mol) is the highest of the four reactions, and closest to the apparent activation energy of DBT pyrolysis (60.68 kcal/mol). Taken together, the activation energy for the formation of DI can be considered to represent that of DBT pyrolysis, and even those of other similar aryl-aryl bonding reactions.

Based on our results and previously published data, we simulated the pyrolysis of DBT and several types of kerogens in a hypothetical 100 Ma source rock that deposits from a surface of 15 °C at a rate of 100 m/Ma along a vertical thermal gradient of 30 °C/km (Fig. 10a, Lewan et al., 2006; Lewan and Ruble, 2002; Vandenbroucke et al., 1999). The correlation between the age of the source rock and temperature can be calculated as $T(°C) = 15+3t(Ma)$ and is considered integrable. The accumulative conversion rate of each organic compound was calculated by reorganizing eq. (1) and eq. (2) to produce eq. (3) below (Lewan and Ruble, 2002):

$$f(X_T) = \ln\frac{1}{1-X_T} = \int A\cdot e^{-\frac{E_a}{RT}}\cdot tdt \quad (3)$$

Table 4
Yields of extracted products from hydrous pyrolysis (m(H_2O):m(DBT) = 100:30) in the temperature range of 400 °C and 500 °C.

Temperature (°C)	Time (h)	DBT Conv. (%)	BP (mg/g)	DI (mg/g)	Ph-DBT (mg/g)	BBBT (mg/g)	MDBT (mg/g)	DMDBT (mg/g)	BT (mg/g)	DBF (mg/g)	FL (mg/g)	Insoluble (mg/g)	S_{org}/C_{org} %	
													Soluble	Insoluble
400	168	0.85	1.17	0.43	0.08	u.d.	Tr	Tr	Tr	Tr	Tr	u.d.	22.0	n.d.
400	408	1.06	1.32	0.19	0.03	u.d.	Tr	Tr	Tr	Tr	Tr	u.d.	22.1	n.d.
420	168	0.99	0.34	0.21	0.04	u.d.	Tr	Tr	Tr	Tr	Tr	u.d.	22.3	n.d.
420	408	12.2	9.61	2.33	0.83	0.06	0.06	0.03	0.22	0.09	0.03	u.d.	22.2	n.d.
450	168	6.20	2.57	0.54	Tr	Tr	Tr	Tr	Tr	Tr	Tr	u.d.	n.d.	n.d.
450	408	23.7	13.2	4.45	3.17	0.38	0.13	0.06	0.43	0.13	0.03	u.d.	21.8	n.d.
480	72	10.8	0.33	6.35	0.52	0.16	0.13	0.02	0.17	0.09	0.03	u.d.	21.0	n.d.
480	168	27.4	11.4	39.3	4.66	1.31	0.22	0.05	0.39	0.10	0.03	u.d.	21.6	n.d.
480	408	45.7	13.5	43.2	8.22	3.28	0.08	0.10	0.54	0.05	0.03	Tr	21.1	n.d.
490	72	1.01	0.75	1.91	0.13	0.01	0.10	0.02	0.03	0.01	0.04	u.d.	21.2	n.d.
490	168	24.1	6.99	22.6	1.84	0.35	0.16	0.03	0.23	0.06	0.03	u.d.	21.7	n.d.
490	336	36.2	14.8	50.6	12.1	6.53	0.43	0.15	0.79	0.06	0.05	u.d.	20.2	n.d.
490	408	60.5	11.8	14.1	19.9	6.00	0.97	0.18	0.81	0.09	0.08	29.9	21.0	19.3
500	72	8.66	2.97	16.1	0.83	0.22	0.11	0.02	0.10	0.05	0.04	6.64	21.0	n.d.
500	168	42.1	11.6	51.6	5.66	2.83	0.23	0.07	0.46	0.07	0.03	u.d.	21.1	n.d.
500	360	74.5	12.7	1.10	15.1	1.50	0.93	0.15	0.82	0.06	0.08	31.3	20.6	18.8

Tr: trace, cannot be quantified; u.d.: under detection limit; n.d: not determined. Soluble represent the organic matters are soluble in DCM. Insoluble represent the organic matters are insoluble in DCM.

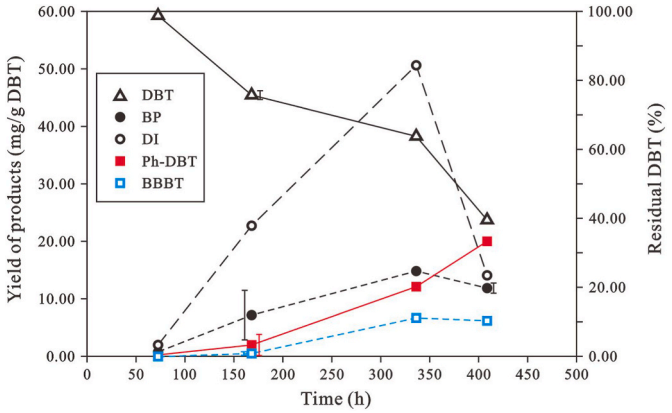

Fig. 2. Yields of representative hydrous-pyrolysis products and the conversion rate of DBT versus time (72–408 h) at 490 °C. The primary Y axis represents the yields of BP, DI, Ph-DBT, and BBBT. The secondary Y axis denotes the percent of the residual weight of DBT. Error bars are next to the symbols.

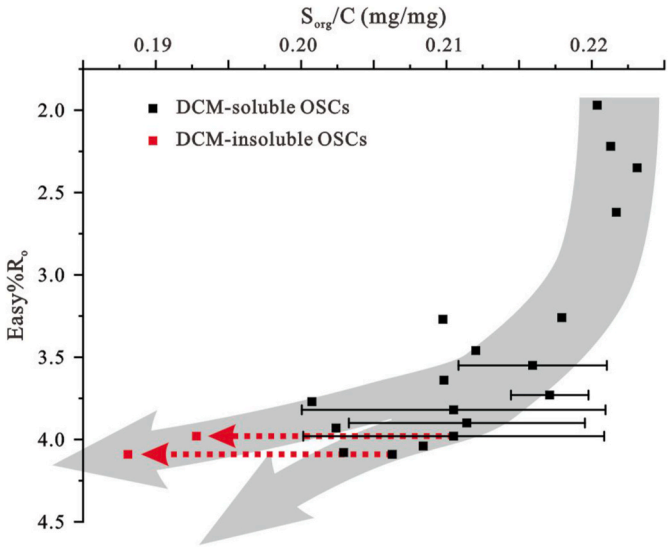

Fig. 3. S_{org}/C_{org} mass ratio of DCM-soluble and DCM-insoluble OSCs of DBT hydrous pyrolysis. m(H_2O):m(DBT) = 100:30.

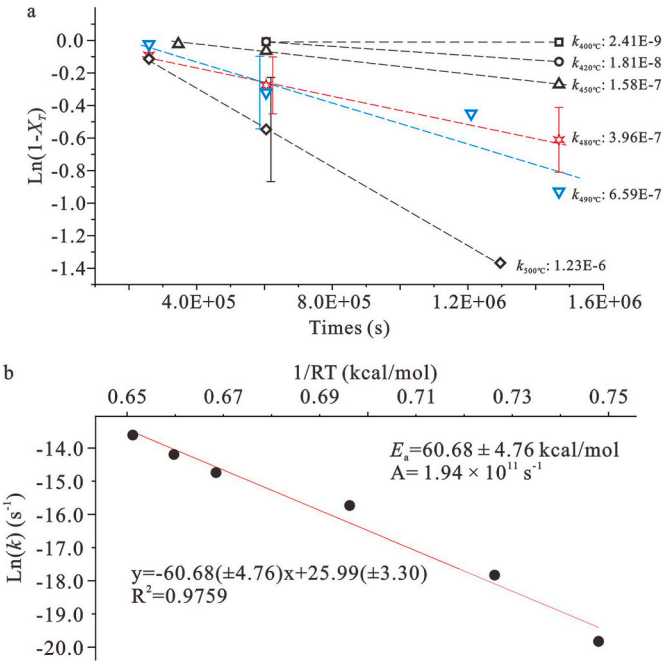

Fig. 4. Determination of the kinetic parameters for the hydrous pyrolysis of DBT with the assumption of a first-order reaction. a) Reaction constants at different temperature; b) Activation energy and pre-log factor determined by the Arrhenius Equation.

Based on our results, the thermal decomposition of kerogens is estimated to occur in a depth range of 1–6 km (Fig. 10b). In comparison, the biaryls are formed in the subsurface region between 6.0 and 8.7 km (195 °C < T < 276 °C), where the corresponding maturity (Easy%R_o) ranges from 2.3% to 3.8%. These data provided kinetic evidence for aryl-aryl coupling in high-maturity organic sediments.

It has been theorised that the thermal maturation of organic compounds in sediments consists essentially of disproportionation reactions in nature (Helgeson et al., 2009). This is consistent with the results of our study indicating that the pyrolysis of DBT consists of its dehydrogenative coupling, which releases hydrogen, and the subsequent hydrocracking of aromatic and heteroaromatic rings. Importantly, our kinetic results demonstrated that aryl-aryl coupling is the rate-limiting step, suggesting that the availability of hydrogen in DBT and other

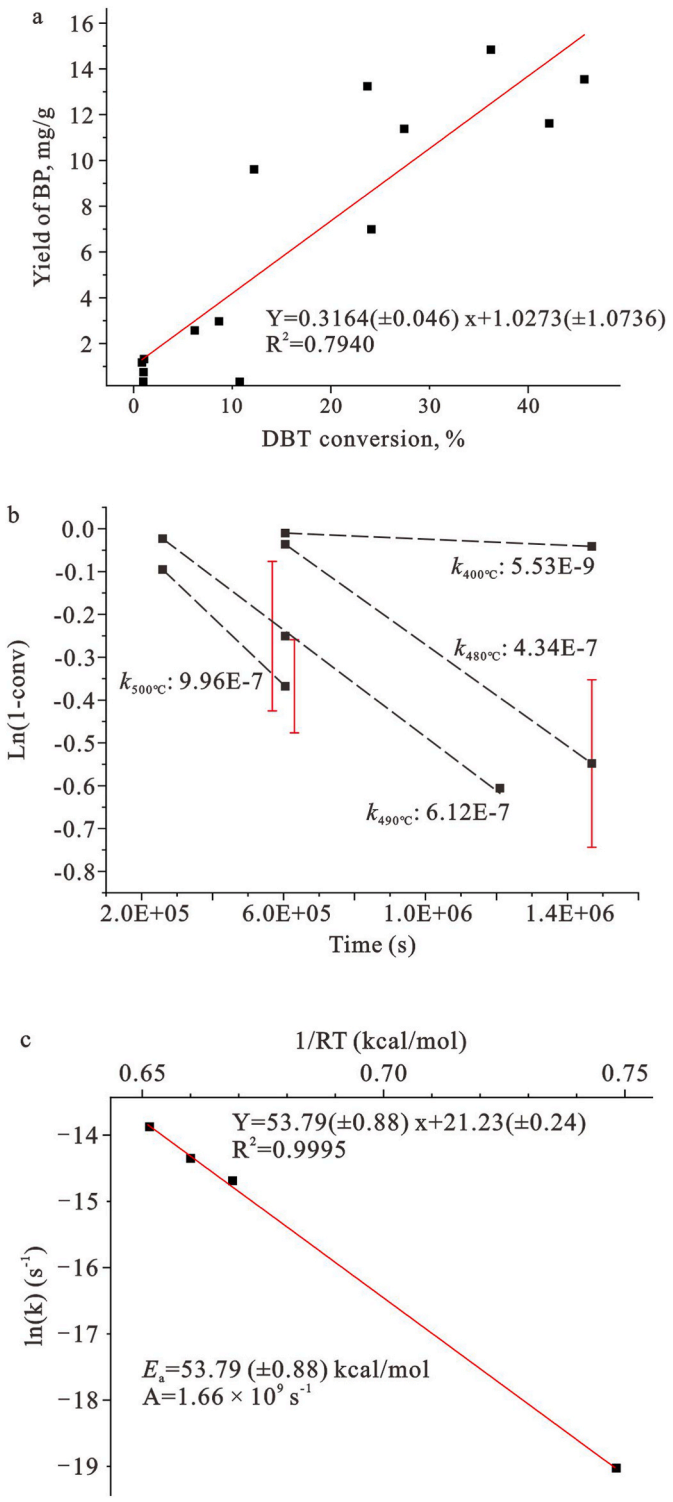

Fig. 5. Kinetic parameters for the generation of BP in this study. a) Yield of BP vs conversion rate of DBT; b) Reaction constants at different T; c) Activation energy and pre-log factor determined by the Arrhenius Equation.

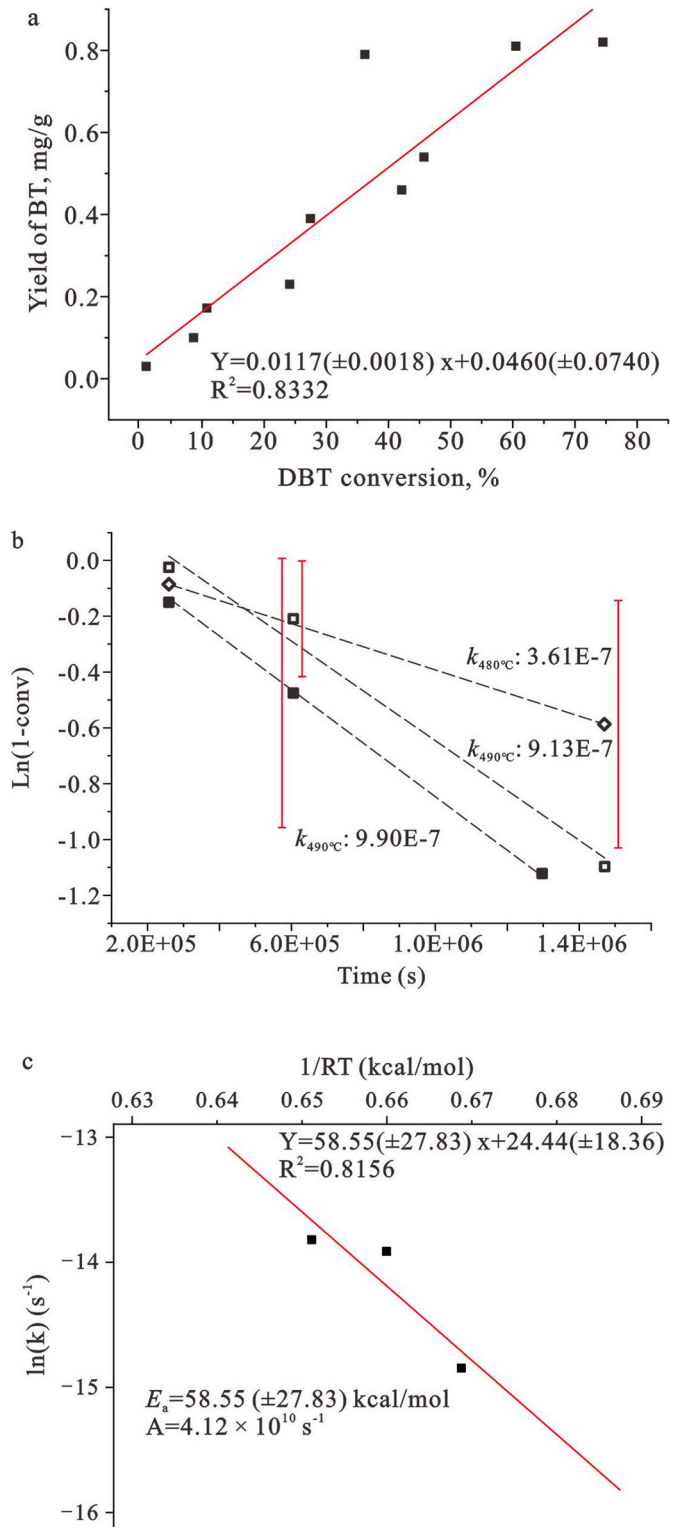

Fig. 6. Kinetic parameters for the generation of BT in this study. a) Yields of BT vs conversion rate of DBT; b) Reaction constants at different T; c) Activation energy and pre-log factor determined by the Arrhenius Equation.

OSCs is a crucial factor in driving their thermal maturation. Indeed, previous thermal simulation studies have shown an inverse correlation between the conversion rate of kerogen and its H/C ratio (Table 6). Taken together, we argue that the pyrolysis of DBT serves as a useful kinetic model for investigating the geochemical behaviour of OSCs in high-maturity sedimentary organic matter, as both share similar H/C ratios.

4.3. Fate of OSCs during thermal maturation

4.3.1. Geochemical behaviour of OSCs during thermal maturation

The fate of OSCs across different vertical strata in the aforementioned hypothetical sedimentary basin is shown in Fig. 11. At the surface level, the sulphurisation of organic compounds is driven mainly by

Table 5
Calculated energy parameters for the coupling of DBT and DBT to form DI, and the coupling of Benzene and DBT to form Ph-DBT.

Configuration	E_0 (Hartree)	ZPE (kcal/mol)	δG (T = 25 °C) (kcal/mol)	E_{sol} (kcal/mol)	$\triangle G$ (Hartree)
Benzene (R)	−232.23	62.92	−15.73	−1.18	−232.15
DBT (R)	−860.29	101.44	−21.43	−3.14	−860.16
2DBT· + 2H· (TS)	−1720.39	199.51	−31.43	−21.11	−1720.12
DBT· + Ph· + 2H·(TS)	−1092.34	161.55	−26.96	−17.15	−1092.12
DI + H_2 (P)	−1720.56	199.35	−31.69	−5.29	−1720.29
Ph-DBT + H_2 (P)	−1092.50	161.17	−27.92	−2.26	−1092.28

E_0, total electron energy; ZPE, zero-point energy; δG, Gibbs' energy at T; E_{sol}, solvation energy, $\triangle G$, Gibbs' energy difference; 1 Hartree = 627.5094 kcal/mol.

biotic mechanisms, such as the assimilatory incorporation of S into cell (Kaplan and Rittenberg, 1964). This is supported by the discovery of sulphate-methane transition (SMT) zones (Borowski et al., 2013; Komada et al., 2016), highly similar trends of sulphur isotope composition between organic matter and inorganic sulphur in the Cariaco Basin of Venezuela (Werne et al., 2003) and cryptic sulphur cycling in oxygen-free waters off the coast of northern Chile (Canfield et al., 2010). Polysulfide cross-linked macromolecules are the main sulphurisation products at this stage, which have been shown to form at temperatures as low as 50 °C in laboratory settings (Amrani et al., 2006). As sedimentation progresses, the increase in pressure and temperature causes chemically labile S–S bonds in OSCs to undergo homolytic cleavage, followed by the formation of C-SH and C–S–C (Fedoseev, 1991). Subsequent cyclisation and structural reorganisation lead to the formation of labile OSCs such as thiolanes and thianes (Damsté et al., 1989; Krein and Aizenshtat, 1995). Microbial sulphate reduction provides the main driving force for the generation of OSCs below 100 °C in marine sediments and crude oils, temperatures that correspond to the region from the surface to ~1000 m subsurface (Anderson and Pratt, 1995; Rueter

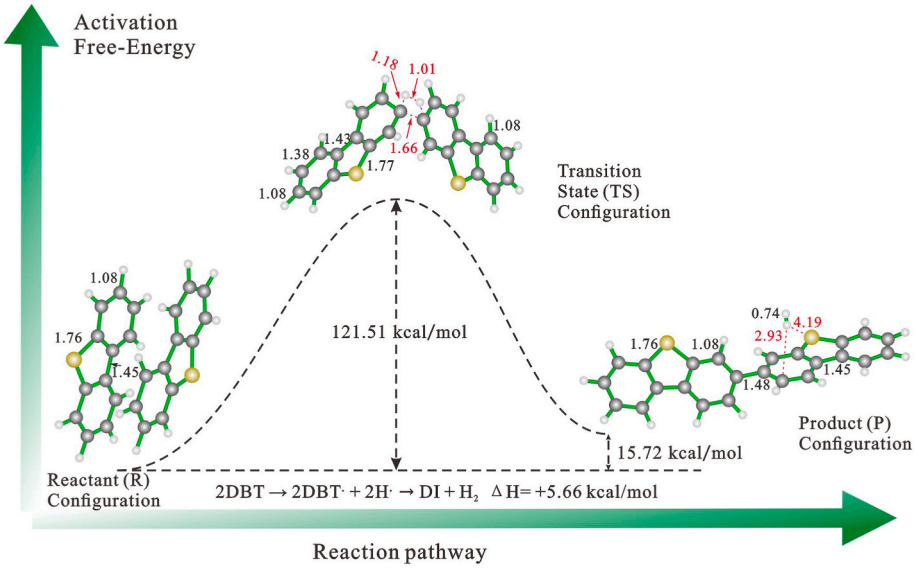

Fig. 7. Geometry and energies of the reactant (R), transition state (TS) and product (P) in the dimerization of DBT. Selected chemical bond lengths (in unit of Å) are also included.

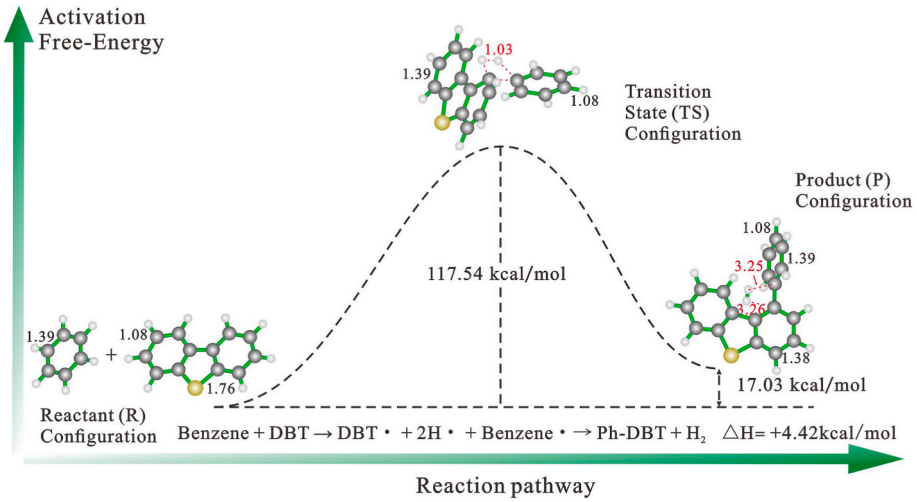

Fig. 8. Geometry and energies of the reactant (R), transition state (TS) and product (P) in the coupling of DBT and benzene. Selected chemical bond lengths (in unit of Å) are also included.

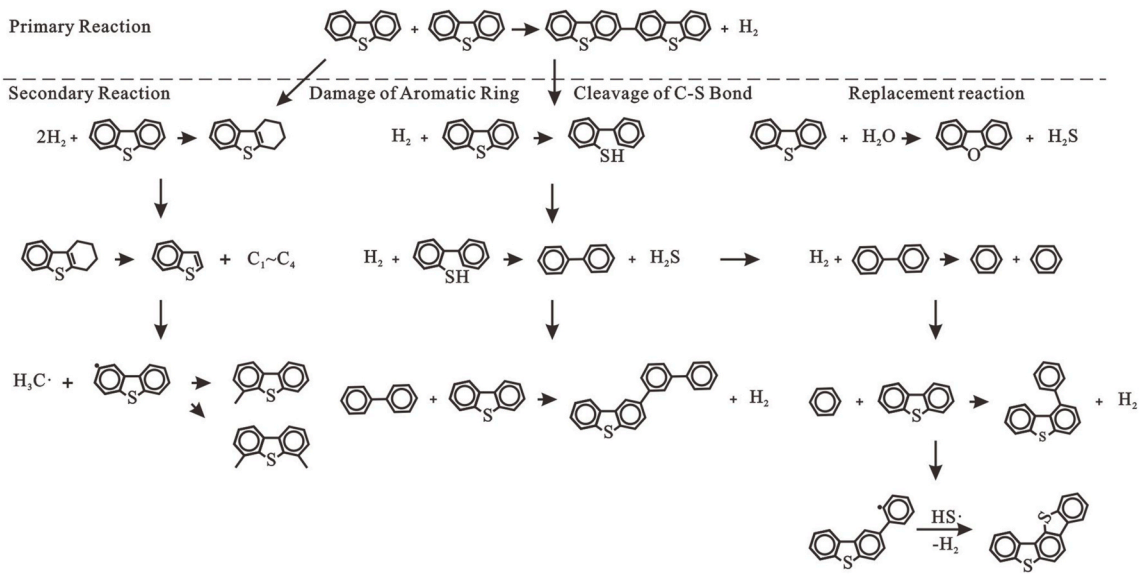

Fig. 9. General scheme of the various reaction pathways contributing to the formation of different DCM-soluble OSCs detected by MS in the current study.

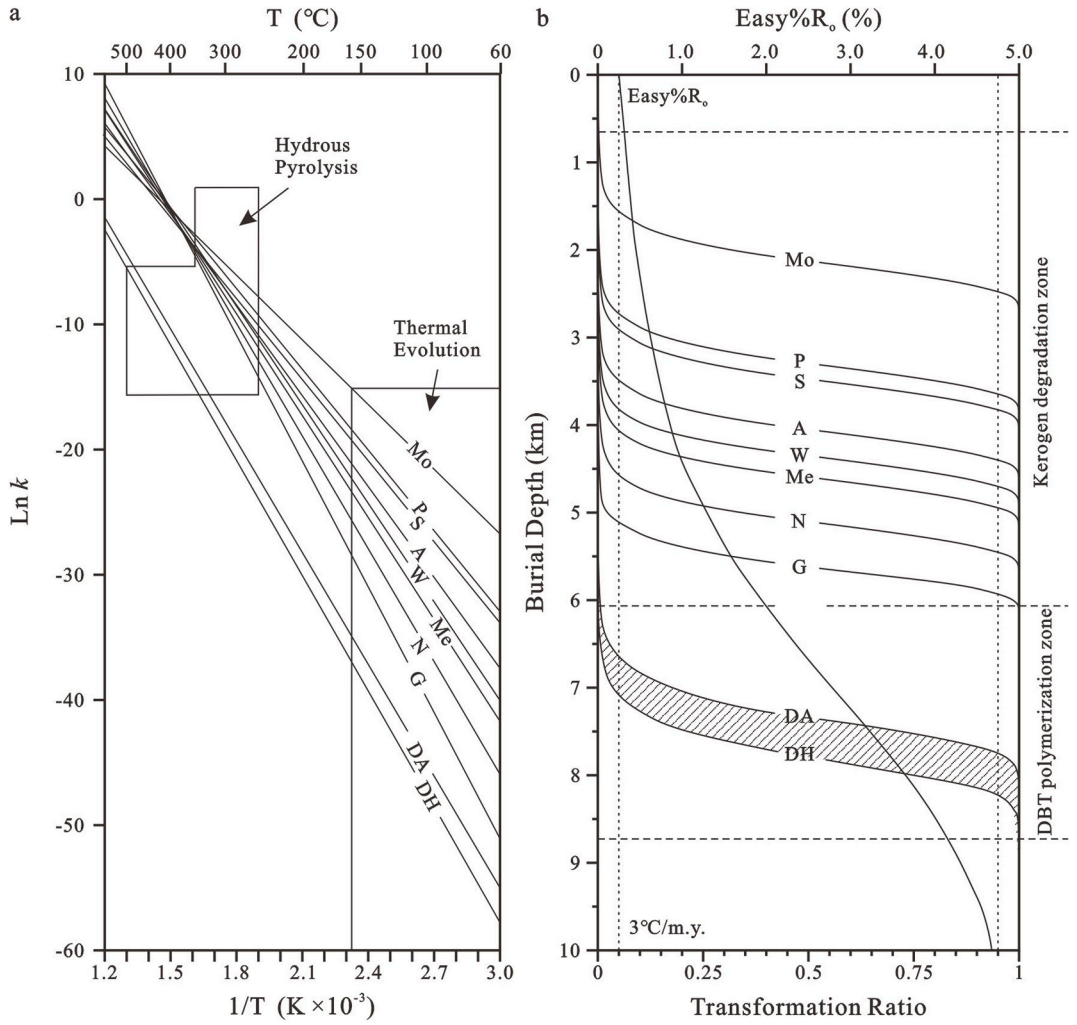

Fig. 10. Kinetics for the polymerisation of DBT and the thermal decomposition of various kerogens. MO: Monterey, P: Phosphoria, S: Menilite shale-IIS, A: Alum shale, W: Woodford, Me: Menilite, N: New Albany, G: Green River, DA: DBT anhydrous, DH: DBT hydrous. a) Arrhenius function plot; b) Evolution curves of petroleum generation and DBT polymerisation based on the assumption of a hypothetical average thermal-burial history. The heating rate is 3 °C/my. Kinetic parameters are based on the results of Lewan et al. (2006), Lewan and Ruble (2002), Dartiguelongue et al. (2006) and this study.

Table 6
Kinetic parameters for the pyrolysis of various kerogens.

Starting materials	E_a (kcal/mol)	A_0 (s^{-1})	H/C Atomic Ratio
Menilite shale-II$_S$	42.78	6.71E+09	1.43
Menilite shale II	53.95	5.04E+13	1.29
Monterey Formation	34.32	2.11E+07	1.25
Phosphoria Retort shale	42.71	1.37E+10	1.20
Alum shale	48.10	4.92E+11	1.11
Woodford Shale	52.16	1.81E+13	1.17
New Albany Shale	59.63	3.79E+15	1.11
Green River Shale	66.63	8.89E+17	1.51
DBT hydrous	60.68	1.94E+11	0.67

Kinetic parameters are based on the results of Lewan et al. (2006), Lewan and Ruble (2002), and this study.

et al., 1994).

At above 100 °C (~3000 m), microbial sulphate reduction gradually subsides and is replaced by TSR. The OSCs are gradually aromatised to form thiophene rings, accompanied by the release of H_2S (Amrani et al., 2005; Orr, 1986; P Koopmans et al., 1998). Simulation experiments have indicated that alkyl thiophenes can form at temperatures as low as 160 °C (Krein and Aizenshtat, 1995). Additionally, H_2S has also been reported to react with alkanes to furnish thiols, thiophenes, and BT (Nguyen et al., 2013). The aromatisation of thiophenes and BT continues with further maturation, leading to structurally more complex OSCs such as DBT.

As the maturity level continues to increase (>6000 m), aryl-aryl coupling becomes more and more prevalent, which is consistent with the detection of biaryl compounds, such as Ph-DBTs, in deep petroleum reservoirs (Li et al., 2012). The released hydrogen subsequently attacks C–S bonds in OSCs and causes the loss of S in the form of H_2S. The organic-derived H_2S can also react with the surrounding minerals to form inorganic sulphides (Cai et al., 2001). These chemical reactions may lead to a steady decline in the S/C ratio (Fig. 3). In our current study, the DCM-soluble and DCM-insoluble OSCs extracted from the pyrolysis products of DBT can be considered to represent crude oils and solid bitumens in hydrocarbon reservoirs, respectively. We found that both types of OSCs were highly desulphurised at the end of their thermal maturation, with the DCM-insoluble OSCs being more desulphurised than their DCM-soluble counterparts (Fig. 3). Because almost all sedimentary organic matter would be converted to solid bitumens at the end of its thermal maturation, OSCs would be buried but could still undergo further disproportionation reactions when temperature and pressure continue to increase.

4.3.2. *Modeling the formation of H_2S from the hydrogenative pyrolysis of OSCs*

It is generally accepted that the S radical-induced thermal decomposition of kerogen plays a key role in petroleum generation (Lewan et al., 2006). During the early phase of pyrolysis, the S/C ratio of the resultant product mixture gradually decreases due to the expulsion of S as H_2S. As kerogen continues to undergo thermal maturation, its S/C ratio would eventually stabilise as the production of H_2S subsides, and the aliphatic sulphuric molecules start to convert to thiophene and other heteroaromatic units. However, the fate of the organic sulphur content during the late-stage of the thermal maturation of kerogen has remained poorly understood. In this regard, our study provides clear evidence that the thermal decomposition of high-maturity kerogen is characterised by further elimination of S as H_2S from its aromatic units, leading to a renewed decline in S/C. These findings suggested that the H_2S in natural gas reservoirs is derived not only from inorganic S compounds via TSR (Li et al., 2012; Zhang et al., 2019), but also from the desulphurisation of organosulphur species such as S-rich kerogen due to their inherent tendency toward dehydrogenation.

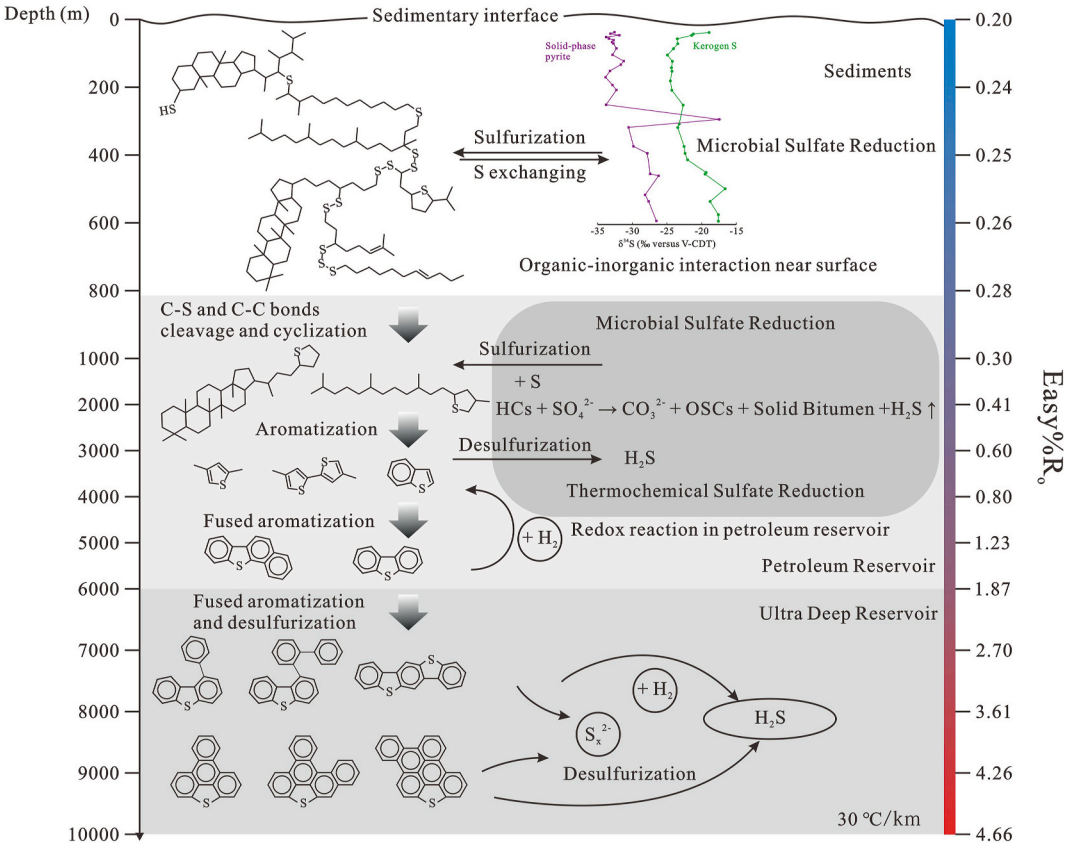

Fig. 11. Fate of organosulphur compounds during the thermal maturation across different vertical strata at a hypothetical heating rate of 3 °C/my. The profile of $\delta^{34}S$ exchange between pyrite sulphur and kerogen sulphur is based on the results of Werne et al. (2003).

In order to further analyse the contribution of OSCs to the generation of H_2S during the thermal maturation of organic matters under high *P-T* conditions, we built a simplified model for the hydrogenative pyrolysis of a generic organosulphur compound with the chemical formula of $C_xH_yS_z$. Early in the metagenesis stage, the organosulphur compound consists exclusively of fused benzene and thiophene rings, with only three types of covalent linkages, C–H, C–C, and C–S. Here, both C–S and C–C bonds are amenable to hydrogenative cleavage, but only the former leads to the formation of H_2S. We further assumed that 1) chemical bonds of the same type (i.e., C–S or C–C) are cleaved at the same probability, with no regioselectivity; 2) hydrogenation shows inherent chemoselectivity between C–S and C–C bonds; and 3) hydrogenation of C–S and C–C bonds is driven by the H_2 endogenously produced from the dehydrogenative condensation of $C_xH_yS_z$.

Based on these three assumptions, the dehydrogenative condensation of $C_xH_yS_z$ to produce H_2 is represented by eq. (4) below:

$$2C_xH_yS_z \rightarrow C_{2x}H_{2y-2}S_{2z} + H_2 \tag{4}$$

The generated H_2 can then either attack C–C bonds, resulting in the fragmentation of a benzene unit and the concomitant formation of butane (eq. (5)), or hydrogenate C–S linkages, releasing S in the form of H_2S from a thiophene ring (eq. (6)).

$$C_xH_yS_z + 3H_2 \xrightarrow{k_1} C_{x-4}H_{y-4}S_z + C_4H_{10} \tag{5}$$

$$C_xH_yS_z + 2H_2 \xrightarrow{k_2} C_xH_{y+2}S_{z-1} + H_2S \tag{6}$$

where k_1 and k_2 are the apparent reaction rate constants for the fragmentation of one benzene and one thiophene unit, respectively. The ratio of k_1 to k_2 thus represents the chemoselectivity of the hydrogenation reaction.

It can be inferred from the above reaction equations that the maximum yield of H_2S (mg/g), designated as $Y_{H_2S}^{max}$, can be achieved when: 1) all $C_xH_yS_z$ molecules are converted and 2) all endogenously generated H_2 is consumed by hydrogenation with either benzene or thiophene units. Obviously, $Y_{H_2S}^{max}$ is controlled by the molar ratio of eq. (5) to eq. (6), denoted by $\frac{M_1}{M_2}$, which is dependent not only on the chemoselectivity of the hydrogenation reaction (k_1/k_2), but also on the stoichiometric ratio of C–C to C–S bonds (denoted by n_1/n_2).

$$\frac{M_1}{M_2} = \frac{k_1}{k_2} \times \frac{n_1}{n_2} \tag{7}$$

For every M_1 moles of eq. (5), there would be M_2 moles of eq. (6). Combined, they will consume M_1+M_2 moles of $C_xH_yS_z$ and $3M_1+2M_2$ moles of H_2, while generating M_2 moles of H_2S. According to eq. (4), $6M_1+4M_2$ moles of $C_xH_yS_z$ are needed to undergo the dehydrogenative coupling to supply the necessary amount of H_2. As a result, the total quantity of $C_xH_yS_z$ that participates in coupling and hydrogenation reactions is calculated to be $7M_1+5M_2$ moles. Based on the above deduction, we can combine eq. (4) with eq. (6) into eq. (8) below.

$$\left(7\frac{M_1}{M_2}+5\right)C_xH_yS_z \rightarrow \left(3\frac{M_1}{M_2}+2\right)C_{2x}H_{2y-2}S_{2z} + \frac{M_1}{M_2}C_4H_{10} + C_xH_{y+2}S_{z-1} + H_2S \tag{8}$$

Eq. (8) thus represents the optimal scenario in which $Y_{H_2S}^{max}$ can be achieved. Based on eq. (8), $Y_{H_2S}^{max}$ can be calculated as follows:

$$Y_{H_2S}^{max} = \frac{34}{\left(7\frac{M_1}{M_2}+5\right) \times (12x + y + 32z)} \times 1000‰ \tag{9}$$

Evidently, solving $Y_{H_2S}^{max}$ requires obtaining the value of $\frac{M_1}{M_2}$, which in turn entails the calculation of k_1/k_2 and n_1/n_2. Based on our assumptions described earlier, each S in $C_xH_yS_z$ must be connected to two C–S bonds. Therefore, the number of C–S bonds in $C_xH_yS_z$ is invariably $n_2 = 2z$. Similarly, the number of C–C bonds in $C_xH_yS_z$ is determined to be $n_1 = \frac{4x-y-2z}{2}$. Therefore, eq. (9) can be rewritten into eq. (10):

$$\frac{M_1}{M_2} = \frac{k_1}{k_2} \times \frac{\left(4 - \frac{y}{x} - 2\frac{z}{x}\right)}{4\frac{z}{x}} \tag{10}$$

In the special case of DBT, eq. (10) can be converted to eq. (11) using the chemical formula of the compound ($C_{12}H_8S$):

$$\frac{M_1}{M_2} = \frac{k_1}{k_2} \times \frac{19}{2} \tag{11}$$

As elucidated earlier, $\frac{M_1}{M_2}$ represents the apparent kinetic ratio of eq. (5) to eq. (6). Therefore, in the case of DBT, $\frac{M_1}{M_2}$ can be calculated using our experimentally obtained kinetic data as follows:

$$\frac{M_1}{M_2}(DBT) = \frac{e^{24.44}e^{\frac{-58.55}{R(T+273.15)}}}{e^{21.23}e^{\frac{-53.79}{R(T+273.15)}}} = \frac{k_1}{k_2} \times \frac{19}{2} \tag{12}$$

where R and T denote the gas constant and the temperature in centigrade, respectively. Therefore, $\frac{k_1}{k_2}$ can be calculated as:

$$\frac{k_1}{k_2} = \frac{2}{19} \times \frac{e^{24.44}e^{\frac{-58.55}{R(T+273.15)}}}{e^{21.23}e^{\frac{-53.79}{R(T+273.15)}}} \tag{13}$$

Combining eq. (10) with eq. (13), we can obtain the formula of $\frac{M_1}{M_2}$ for any generic $C_xH_yS_z$:

$$\frac{M_1}{M_2} = \frac{2}{19} \times \frac{e^{24.44}e^{\frac{-58.55}{R(T+273.15)}}}{e^{21.23}e^{\frac{-53.79}{R(T+273.15)}}} \times \frac{\left(4 - \frac{y}{x} - 2\frac{z}{x}\right)}{4\frac{z}{x}} \tag{14}$$

Therefore, $Y_{H_2S}^{max}$ can be calculated by combining eq. (9) and eq. (14). It is evident that the maximum yield of H_2S is governed by temperature and the average atomic composition of the organosulphur species. To facilitate the calculation of eq. (9), we set x to 35 according to previously reported estimates on the average number of carbons in natural-occurring organic compounds (Rathsack et al., 2014; Walters et al., 2015). As a result, eq. (9) can be simplified as follows:

$$Y_{H_2S}^{max} = \frac{34}{\left(18.26 \times e^{\frac{-4.76}{R(T+273.15)}} \times \frac{4 - \frac{y}{x} - 2\frac{z}{x}}{4\frac{z}{x}} + 5\right) \times \left(420 + 35\frac{y}{x} + 1120\frac{z}{x}\right)} \tag{15}$$

To illustrate this, we generated slices of a 4D map based on H/C (y/x), S/C (z/x), and T (Fig. 12). This mathematical model can provide a convenient tool to estimate the contribution of high-maturity OSCs to H_2S formation in sedimentary petroleum basins. Furthermore, the yield of C_4H_{10} can be calculated following the same method:

$$Y_{C_4H_{10}}^{max} = \frac{151.28 \times e^{\frac{-4.76}{R(T+273.15)}} \times \frac{4 - \frac{y}{x} - 2\frac{z}{x}}{4\frac{z}{x}}}{\left(18.26 \times e^{\frac{-4.76}{R(T+273.15)}} \times \frac{4 - \frac{y}{x} - 2\frac{z}{x}}{4\frac{z}{x}} + 5\right) \times \left(420 + 35\frac{y}{x} + 1120\frac{z}{x}\right)} \tag{16}$$

4.3.3. Estimation of the level of organosulphur-derived H_2S in the Sichuan Basin

Previous geological prospections have led to the discovery of large dolomitic natural gas in Sinian reservoirs with high levels of hydrogen sulphide and S-rich asphaltenes in the Gaoshiti-Moxi region of Sichuan Basin. These reservoirs had apparently undergone thermal maturation under high *P-T* conditions (~3% R_o; Liu et al., 2018; Yang et al., 2018; Zhang et al., 2019). We thus intended to use our model to estimate the level of H_2S released from the solid bitumens in the dolomite reservoirs

in the Dengying Formation (Z_2dn^2, 541–600 Ma) of the central Sichuan uplift. As the thermal maturation of the S-rich solid bitumen and the generation of H_2S are both cumulative events, the total amount of H_2S can be calculated by finding the integral of fractional yields over the period of heating time. In each time segment, we reasoned that the corresponding maximum yield of H_2S can be expressed as:

$$Y(t) = X(t) \times Y_{H_2S}^{max}(t) \tag{17}$$

where X(t) and $Y_{H_2S}^{max}(t)$ are the conversion rate of dehydrogenation from aryl-aryl coupling and the maximum yield of H_2S at time t, respectively.

Finally, the correlation between T and t can be obtained from the thermal history of the Dengying Formation at Well MX9, which was characterised and published in a previous study (see Fig. 13; Liu et al., 2018). As elucidated in section 4.2, we considered the kinetic parameters of aryl-aryl condensation to be largely unaffected by various aromatic organic compounds at high maturity. Therefore, we used the activation energy (60.68 kcal/mol) and frequency factor (1.94×10^{11} s^{-1} = 6.12×10^{24} Ma^{-1}) of DBT dimerisation to represent those of generic aryl-aryl coupling. Taken together, X(t) can be re-expressed as a function of time as below:

$$X(t) = 1 - \frac{1}{exp\left(t \times (6.12E+24) \times exp\left(-\frac{60.68}{R(T(t)+273.15)}\right)\right)} \tag{18}$$

where t represents the heating time in Ma and T(t) is the temperature of the Dengying Formation at time t.

$Y_{H_2S}^{max}$ can also be re-expressed as a function of time and the average atomic composition of organosulphur species based on the published thermal history and eq. (15). According to Zhang et al. (2019), the current chemical formula of S-rich solid bitumen in the Sinian reservoirs of the Gaoshiti-Moxi region roughly corresponded to $CH_{0.5}S_{0.06}$. However, the H/C and S/C atomic ratios represent the element composition of the product, which has experienced thermochemical alternation. It is necessary to reconstruct H/C and S/C atomic ratios with the constraint of this model. In each time segment, the initial H/C and S/C can be determined from the yields of H_2S and C_4H_{10}, as well as the H/C and S/C of organic OSC products as follows:

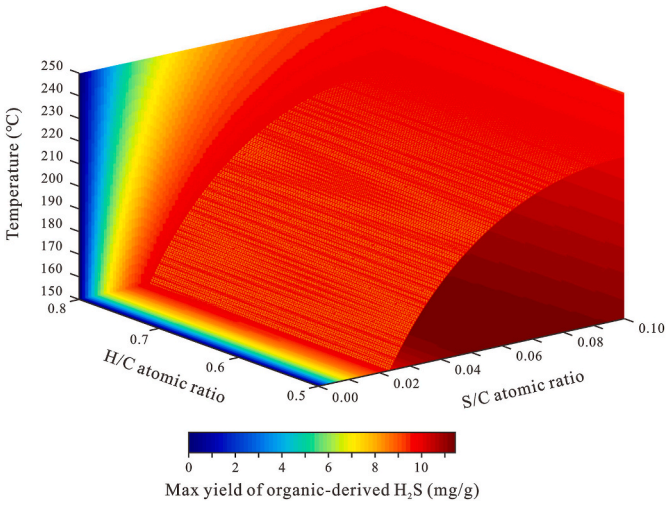

Fig. 12. Maximum yield of organic-derived H_2S constrained by S/C atomic ratios (0.01–0.10), H/C atomic ratios (0.50–0.80), and temperature (150–250 °C) in sedimentary organic systems. The contour surface indicates the maximum yield of organic-derived H_2S at 10 mg/g.

adopted a trial-and-error approach by experimenting with different initial H/C and S/C at t = 150 Ma and then iteratively calculating the yields of C_4H_{10} and H_2S in each period. This allowed us to obtain the hypothetical final H/C and S/C of the solid bitumens at present (t = 0). By matching the calculation with the experimentally determined H/C and S/C values, we obtained the H/C, S/C, and Y_{H_2S} for each period. Finally, $Y_{H_2S}^{total}$ was calculated to be 1.58 mg/g by adding Y_{H_2S} in all time periods together.

The results above strongly support an OSC contribution to the generation of abiotic H_2S in ultra-deep petroleum reservoirs, particular during the late stage of thermal maturation. However, the low yield of organic-derived H_2S can easily be scavenged by surrounding minerals to form inorganic sulphides. The large scale accumulation of organic-derived H_2S must be triggered by external hydrogen sources, such as hydrothermal fluids or water-rock reactions. Overall, we consider

$$H/C = \frac{\left(7\frac{M_1}{M_2}+5\right)\times\left(35\frac{y}{x}\right) - Y_{H_2S}\times\left(7\frac{M_1}{M_2}+5\right)\times\left(420+35\frac{y}{x}+1120\frac{z}{x}\right)\times\frac{2}{34} - Y_{C_4H_{10}}\times\left(7\frac{M_1}{M_2}+5\right)\times\left(420+35\frac{y}{x}+1120\frac{z}{x}\right)\times\frac{10}{58}}{\left(7\frac{M_1}{M_2}+5\right)\times 420 - Y_{C_4H_{10}}\times\left(7\frac{M_1}{M_2}+5\right)\times\left(420+35\frac{y}{x}+1120\frac{z}{x}\right)\times\frac{48}{58}}\times 12 \tag{19}$$

$$S/C = \frac{\left(7\frac{M_1}{M_2}+5\right)\times\left(1120\frac{z}{x}\right) - Y_{H_2S}\times\left(7\frac{M_1}{M_2}+5\right)\times\left(420+35\frac{y}{x}+1120\frac{z}{x}\right)\times\frac{32}{34}}{\left(7\frac{M_1}{M_2}+5\right)\times 420 - Y_{C_4H_{10}}\times\left(7\frac{M_1}{M_2}+5\right)\times\left(420+35\frac{y}{x}+1120\frac{z}{x}\right)\times\frac{48}{58}}\times\frac{12}{32} \tag{20}$$

As we intended to focus on the metagenesis stage of the thermal maturation of S-rich solid bitumens, the upper and lower bounds of the integral were set to 0 and 150 (Ma), respectively.

$$Y_{H_2S}^{total} = \int_0^{150} X(t)\cdot Y_{H_2S}^{max}(t)dt \tag{21}$$

To calculate $Y_{H_2S}^{total}$, we divided the total time (i.e., 150 Ma) into 133 equal periods and assumed that i) temperature remained constant in each periods and ii) the release of C_4H_{10} and H_2S led to slight but non-negligible changes in H/C and S/C. Based on these considerations, we

organic matter in sedimentary petroleum basins to serve as a carrier that transports inorganic sulphur from surface regions to deep strata which is in good agreement with Ho et al. (1974).

5. Conclusion

The data that we obtained from the hydrous pyrolysis of DBT in gold-tube simulation experiments under high *P-T* conditions provided valuable insights into the geochemical behaviour of OSCs during the advanced stage of thermal maturation. We also determined the kinetic parameters of DBT pyrolysis both experimentally and by theoretical calculation via DFT. These results suggested that the thermal maturation

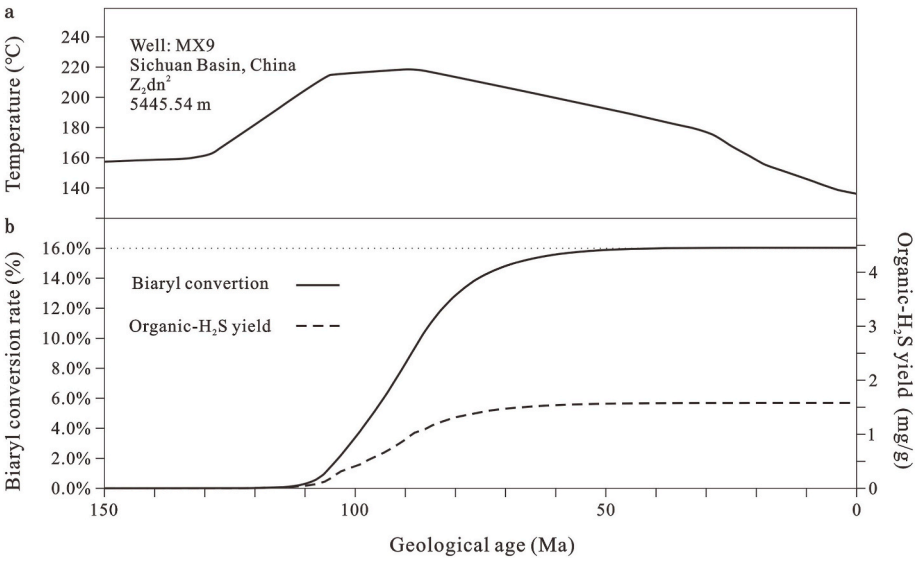

Fig. 13. Model prediction of the yield of organic-derived H_2S from S-rich solid bitumens in the Sichuan Basin (b). The thermal history of the Dengying Formation (Z_2dn^2) in the Gaoshiti-Moxi region, Sichuan Basin, is modified after Liu et al. (2018) (a).

of OSCs is an extremely complex process. Key reactions that drive OSC pyrolysis include dehydronative aryl-aryl coupling, which is rate-limiting, and hydrogenative cleavage of C–C, C–H, and C–S bonds, leading to the fragmentation of aromatic and heterocyclic aromatic compounds. Dehydrogenative aryl-aryl coupling mainly occurred in the Easy%R_o range of 2.3%–3.8% (190–270 °C) and showed an activation energy of approximately 60 kcal/mol. The present study provided convincing evidence that OSCs are key contributors to the accumulation of sulphides in ultra-deep petroleum reservoirs, particularly when the organic sediments are at the late stage of their thermal maturation (i.e., metagenesis). Near the surface, inorganic sulphur is incorporated into various organic compounds via microbial sulphate reduction, and the resultant OSCs are deposited to deeper strata through sedimentation, where they are hydrocracked under high *P-T* conditions to release H_2S. The geochemical behaviour of OSCs predicted from our model not only provided important insights into the H_2S generation potential of over-mature sedimentary organic matter, but it could also serve as a useful guide for estimating the level of external hydrogen that participate in the thermal maturation of OSCs.

Author contributions

Project concept and experiment design was proposed by Jia Wu. Pyrolysis experimental work and quantum chemistry calculation was conducted by Xiao Jin and Peng Fang. Calculation of Easy%R_o and modeling was finished by Jia Wu and Xiao Jin. Zhihuan Zhang, Meijun Li and Ningning Zhong conceived of and supervised the project. All the authors contributed to the manuscript.Jia Wu: Project Concept and experiment design, Modelling, Xiao Jin: Pyrolysis experimental work, Easy%Ro calculation, Modelling, Peng Fang: Quantum chemistry calculation, Zhihuan Zhang: Supervision of the project, Meijun Li: Supervision of the project, Ningning Zhong: Supervision of the project

Declaration of competing interest

The authors declare that they have no known competing financial interests or personal relationships that could have appeared to influence the work reported in this paper.

Acknowledgments

We would like to thank the reviewers for their helpful comments suggestions, scientific and linguistic revisions of the manuscript. In addition, the authors are grateful for the assistance of Lei Zhu, Shengbao Shi and Shuo Gao for all the experiments. High Performance Computing Center, Sichuan University of Science & Engineering is acknowledged for providing computational. We acknowledge Steve Larter, Haiping Huang and Keya Zhang for their comments on early versions of this paper. This research was supported by National Key Research and Development Program of China (Grant No. 2017YFC0603102), National Natural Science Foundation of China (No.41403049), the Foundation of State Key Laboratory of Petroleum Resources and Prospecting, China University of Petroleum (Beijing) (No. PRP/indep-3-1715) and China Scholarship Council (No.201906440182). At last, the first author Xiao Jin would like to thank the patience, care and suppor from Yinan He as a companion all the way and would you please marry him?

Appendix

Table A
Yields of selected products at 450 °C for 4 days in anhydrous and aquatic media.

mH_2O: mDBT	Anhydrous	10:1
BP (mg/g DBT)	3.10	6.00
BT (mg/g DBT)	0.11	0.13
DBF (mg/g DBT)	9.14×10^{-3}	6.31×10^{-2}
Ph-DBT (mg/g DBT)	0.32	0.06
FL (mg/g DBT)	0.06	0.05
MDBT (mg/g DBT)	0.39	0.11
DMDBT (mg/g DBT)	0.06	0.01

References

Amrani, A., 2014. Organosulfur compounds: molecular and isotopic evolution from biota to oil and gas. Annu. Rev. Earth Planet Sci. 42, 733–768.

Amrani, A., Aizenshtat, Z., 2004. Reaction of polysulfide anions with α,β unsaturated isoprenoid aldehydes in aquatic media: simulation of oceanic conditions. Org. Geochem. 35, 909–921.

Amrani, A., Said-Ahamed, W., Aizenshtat, Z., 2005. The δ34S values of the early-cleaved sulfur upon low temperature pyrolysis of a synthetic polysulfide cross-linked polymer. Org. Geochem. 36, 971–974.

Amrani, A., Said-Ahamed, W., Lewan, M.D., Aizenshtat, Z., 2006. Experiments on δ34S mixing between organic and inorganic sulfur species during thermal maturation. Geochem. Cosmochim. Acta 70, 5146–5161.

Amrani, A., Deev, A., Sessions, A.L., Tang, Y., Adkins, J.F., Hill, R.J., Moldowan, J.M., Wei, Z., 2012. The sulfur-isotopic compositions of benzothiophenes and dibenzothiophenes as a proxy for thermochemical sulfate reduction. Geochem. Cosmochim. Acta 84, 152–164.

Anderson, T., Pratt, L., 1995. Isotopic Evidence for the Origin of Organic Sulfur and Elemental Sulfur in Marine Sediments, pp. 378–396.

Asif, M., Alexander, R., Fazeelat, T., Pierce, K., 2009. Geosynthesis of dibenzothiophene and alkyl dibenzothiophenes in crude oils and sediments by carbon catalysis. Org. Geochem. 40, 895–901.

Birdwell, J.E., Lewan, M.D., Bake, K.D., Bolin, T.B., Craddock, P.R., Forsythe, J.C., Pomerantz, A.E., 2018. Evolution of sulfur speciation in bitumen through hydrous pyrolysis induced thermal maturation of Jordanian Ghareb Formation oil shale. Fuel 219, 214–222.

Borowski, W.S., Rodriguez, N.M., Paull, C.K., Ussler, W., 2013. Are 34S-enriched authigenic sulfide minerals a proxy for elevated methane flux and gas hydrates in the geologic record? Mar. Petrol. Geol. 43, 381–395.

Cai, C., Hu, W., Worden, R.H., 2001. Thermochemical sulphate reduction in cambro–ordovician carbonates in central tarim. Mar. Petrol. Geol. 18, 729–741.

Cai, C., Zhang, C., Cai, L., Wu, G., Jiang, L., Xu, Z., Li, K., Ma, A., Chen, L., 2009. Origins of palaeozoic oils in the tarim basin: evidence from sulfur isotopes and biomarkers. Chem. Geol. 268, 197–210.

Canfield, D.E., Stewart, F.J., Thamdrup, B., De Brabandere, L., Dalsgaard, T., Delong, E. F., Revsbech, N.P., Ulloa, O., 2010. A cryptic sulfur cycle in oxygen-minimum–zone waters off the Chilean coast. Science 330, 1375.

Chakhmakhchev, A., Suzuki, M., Takayama, K., 1997. Distribution of alkylated dibenzothiophenes in petroleum as a tool for maturity assessments. Org. Geochem. 26, 483–489.

Damsté, J.S.S., Koert, E.R.V., Dalen, K.V., Leeuw, J.W.D., Schenck, P.A., 1989. Characterisation of highly branched isoprenoid thiophenes occurring in sediments and immature crude oils. Org. Geochem. 14, 0–567.

Dartiguelongue, C., Behar, F., Budzinski, H., Scacchi, G., Marquaire, P.M., 2006. Thermal stability of dibenzothiophene in closed system pyrolysis: experimental study and kinetic modelling. Org. Geochem. 37, 98–116.

Ellis, G.S., Said-Ahmad, W., Lillis, P.G., Shawar, L., Amrani, A., 2017. Effects of thermal maturation and thermochemical sulfate reduction on compound-specific sulfur isotopic compositions of organosulfur compounds in Phosphoria oils from the Bighorn Basin, USA. Org. Geochem. 103, 63–78.

Fang, R., Wang, T.G., Li, M., Xiao, Z., Zhang, B., Huang, S., Shi, S., Wang, D., Deng, W., 2016. Dibenzothiophenes and benzo[b]naphthothiophenes: molecular markers for tracing oil filling pathways in the carbonate reservoir of the Tarim Basin, NW China. Org. Geochem. 91, 68–80.

Fedoseev, V.M., 1991. ChemInform abstract: investigation of organic reactions by the use of radioactive sulfur. ChemInform 22.

Greenwood, P.F., Mohammed, L., Grice, K., McCulloch, M., Schwark, L., 2018. The application of compound-specific sulfur isotopes to the oil–source rock correlation of Kurdistan petroleum. Org. Geochem. 117, 22–30.

Grosjean, E., Love, G.D., Stalvies, C., Fike, D.A., Summons, R.E., 2009. Origin of petroleum in the neoproterozoic–cambrian South Oman Salt Basin. Org. Geochem. 40, 87–110.

Guan, S., Zhang, C., Ren, R., Zhang, S., Wu, L., Wang, L., Ma, P., Han, C., 2019. Early Cambrian syndepositional structure of the northern Tarim Basin and a discussion of Cambrian subsalt and deep exploration. Petrol. Explor. Dev. 46, 1141–1152.

He, K., Zhang, S., Mi, J., Zhang, W., 2018. The evolution of chemical groups and isotopic fractionation at different maturation stages during lignite pyrolysis. Fuel 211, 492–506.

Helgeson, H.C., Richard, L., McKenzie, W.F., Norton, D.L., Schmitt, A., 2009. A chemical and thermodynamic model of oil generation in hydrocarbon source rocks. Geochem. Cosmochim. Acta 73, 594–695.

Ho, T.Y., Rogers, M.A., Drushel, H.V., Koons, C.B., 1974. Evolution of sulfur compounds in crude oils. AAPG Bull. 58, 2338–2348.

Hughes, W.B., Holba, A.G., Dzou, L.I.P., 1995. The ratios of dibenzothiophene to phenanthrene and pristane to phytane as indicators of depositional environment and lithology of petroleum source rocks. Geochem. Cosmochim. Acta 59, 3581–3598.

Kaplan, I., Rittenberg, S., 1964. Microbiological fractionation of sulphur isotopes. Jorunal of General Microbiology 34, 195–212.

Kelemen, S.R., Walters, C.C., Kwiatek, P.J., Freund, H., Afeworki, M., Sansone, M., Lamberti, W.A., Pottorf, R.J., Machel, H.G., Peters, K.E., Bolin, T., 2010. Characterization of solid bitumens originating from thermal chemical alteration and thermochemical sulfate reduction. Geochem. Cosmochim. Acta 74, 5305–5332.

Klimova, T.E., Valencia, D., Mendoza-Nieto, J.A., Hernández-Hipólito, P., 2013. Behavior of NiMo/SBA-15 catalysts prepared with citric acid in simultaneous hydrodesulfurization of dibenzothiophene and 4,6-dimethyldibenzothiophene. J. Catal. 304, 29–46.

Komada, T., Burdige, D.J., Li, H.-L., Magen, C., Chanton, J.P., Cada, A.K., 2016. Organic matter cycling across the sulfate-methane transition zone of the Santa Barbara Basin, California Borderland. Geochem. Cosmochim. Acta 176, 259–278.

P Koopmans, M., Rijpstra, I., Leeuw, J.W., Lewan, M., Sinninghe-Damste, J., 1998. Artificial Maturation of an Immature Sulfur- and Organic Matter-Rich Limestone from the Ghareb Formation, Jordan.

Krein, E., Aizenshtat, Z., 1995. Proposed thermal pathways for sulfur transformations in organic macromolecules. Laboratory Simulation Experiments 110–137.

Lee, R.Z., Ng, F.T.T., 2006. Effect of water on HDS of DBT over a dispersed Mo catalyst using in situ generated hydrogen. Catal. Today 116, 505–511.

Lewan, M.D., 1997. Experiments on the role of water in petroleum formation. Geochem. Cosmochim. Acta 61, 3691–3723.

Lewan, M.D., Ruble, T.E., 2002. Comparison of petroleum generation kinetics by isothermal hydrous and nonisothermal open-system pyrolysis. Org. Geochem. 33, 1457–1475.

Lewan, M.D., Kotarba, M.J., Curtis, J.B., Więcław, D., Kosakowski, P., 2006. Oil-generation kinetics for organic facies with type-II and -IIS kerogen in the menilite shales of the polish carpathians. Geochem. Cosmochim. Acta 70, 3351–3368.

Li, M., Wang, T.G., Simoneit, B.R.T., Shi, S., Zhang, L., Yang, F., 2012. Qualitative and quantitative analysis of dibenzothiophene, its methylated homologues, and benzonaphthothiophenes in crude oils, coal, and sediment extracts. J. Chromatogr. A 1233, 126–136.

Li, S., Shi, Q., Pang, X., Zhang, B., Zhang, H., 2012. Origin of the unusually high dibenzothiophene oils in Tazhong-4 Oilfield of Tarim Basin and its implication in deep petroleum exploration. Org. Geochem. 48, 56–80.

Li, M.J., Wang, T.G., Zhong, N.N., Zhang, W.B., Sadik, A., Li, H.B., 2013. Ternary diagram of fluorenes, dibenzothiophenes and dibenzofurans: indicating depositional environment of crude oil source rocks. Energy Explor. Exploit 31, 569–588.

Li, M., Wang, T.G., Shi, S., Liu, K., Ellis, G.S., . Benzo[b]naphthothiophenes and alkyl dibenzothiophenes: molecular tracers for oil migration distances. Mar. Petrol. Geol. 57, 403–417.

Li, Y., Chen, S., Wang, Y., Su, K., He, Q., Qiu, W., Xiao, Z., 2020. Relationships between hydrocarbon evolution and the geochemistry of solid bitumen in the Guanwushan Formation, NW Sichuan Basin. Mar. Petrol. Geol. 111, 116–134.

Liu, W., Qiu, N., Xu, Q., Liu, Y., 2018. Precambrian temperature and pressure system of Gaoshiti-Moxi block in the central paleo-uplift of Sichuan Basin, southwest China. Precambrian Res. 313, 91–108.

Machel, H., 2006. Bacterial and Thermochemical Sulfate Reduction in Diagenetic Settings - Old and New Insights, Agu Fall Meeting.

McCollom, T.M., Seewald, J.S., German, C.R., 2015. Investigation of extractable organic compounds in deep-sea hydrothermal vent fluids along the Mid-Atlantic Ridge. Geochem. Cosmochim. Acta 156, 122–144.

Nguyen, V.P., Burklé-Vitzthum, V., Marquaire, P.M., Michels, R., 2013. Thermal reactions between alkanes and H2S or thiols at high pressure. J. Anal. Appl. Pyrol. 103, 307–319.

Orr, W.L., 1986. Kerogen/asphaltene/sulfur Relationships in Sulfur-Rich Monterey Oils.

Radke, M., 1988. Application of aromatic compounds as maturity indicators in source rocks and crude oils. Mar. Petrol. Geol. 5, 224–236.

Radke, M., Vriend, S.P., Ramanampisoa, L.R., 2000. Alkyldibenzofurans in terrestrial rocks: influence of organic facies and maturation. Geochem. Cosmochim. Acta 64, 275–286.

Rathsack, P., Kroll, M.M., Otto, M., 2014. Analysis of high molecular compounds in pyrolysis liquids from a German brown coal by FT-ICR-MS. Fuel 115, 461–468.

Reckendorf, R.M.Z., 2000. Phenyl-substituted polycyclic aromatic compounds as intermediate products during pyrolytic reactions involving coal tars, pitches and related materials. Chromatographia 52, 67–76.

Rospondek, M.J., Szczerba, M., Malek, K., Góra, M., Marynowski, L., 2008. Comparison of phenyldibenzothiophene distributions predicted from molecular modelling with relevant experimental and geological data. Org. Geochem. 39, 1800–1815.

Rueter, P., Rabus, R., Wilkest, H., Aeckersberg, F., Rainey, F.A., Jannasch, H.W., Widdel, F., 1994. Anaerobic oxidation of hydrocarbons in crude oil by new types of sulphate-reducing bacteria. Natur 372, 455–458.

Santamaria-Orozco, D., Horsfield, B., di Primio, R., Welte, D.H., 1998. Influence of maturity on distributions of benzo- and dibenzothiophenes in Tithonian source rocks and crude oils, Sonda de Campeche, Mexico. Org. Geochem. 28, 423–439.

Schoenherr, J., Littke, R., Urai, J., Kukla, P., Rawahi, Z., 2007. Polyphase thermal evolution in the Infra-Cambrian Ara Group (South Oman Salt Basin) as deduced by solid bitumen maturity. Org. Geochem. 38, 1293–1318.

Shi, S., Li, M., Lei, Z., 2014. Identification and distribution of C1-and C2-alkylated dibenzothiophenes in petroleum and sedimentary organic matter. Petroleum Geology & Experiment.

Song, D., Zhang, C., Li, S., Wang, T.G., Li, M., 2017. Elevated mango's K1 values resulting from thermochemical sulfate reduction within the tazhong oils, tarim basin. Energy Fuels 31, 1250–1258.

Sweeney, J.J., Burnham, A.K., 1990. Evaluation of a simple model of vitrinite reflectance based on Chemical kinetics. AAPG Bull. 74, 1559–1570.

Vandenbroucke, M., Behar, F., Rudkiewicz, J.L., 1999. Kinetic modelling of petroleum formation and cracking: implications from the high pressure/high temperature Elgin Field (UK, North Sea). Org. Geochem. 30, 1105–1125.

Wacey, D., Noffke, N., Cliff, J., Barley, M.E., Farquhar, J., 2015. Micro-scale quadruple sulfur isotope analysis of pyrite from the ~3480Ma Dresser Formation: new insights into sulfur cycling on the early Earth. Precambrian Res. 258, 24–35.

Walters, C.C., Wang, F.C., Qian, K., Wu, C., Mennito, A.S., Wei, Z., 2015. Petroleum alteration by thermochemical sulfate reduction – a comprehensive molecular study of aromatic hydrocarbons and polar compounds. Geochem. Cosmochim. Acta 153, 37–71.

Werne, J.P., Lyons, T.W., Hollander, D.J., Formolo, M.J., Sinninghe Damsté, J.S., 2003. Reduced sulfur in euxinic sediments of the Cariaco Basin: sulfur isotope constraints on organic sulfur formation. Chem. Geol. 195, 159–179.

Yang, C., Ni, Z., Li, M., Wang, T., Chen, Z., Hong, H., Tian, X., 2018. Pyrobitumen in South China: organic petrology, chemical composition and geological significance. Int. J. Coal Geol. 188, 51–63.

Zhang, T., Ellis, G.S., Wang, K.-s., Walters, C.C., Kelemen, S.R., Gillaizeau, B., Tang, Y., 2007. Effect of hydrocarbon type on thermochemical sulfate reduction. Org. Geochem. 38, 897–910.

Zhang, S., Mi, J., He, K., 2013. Synthesis of hydrocarbon gases from four different carbon sources and hydrogen gas using a gold-tube system by Fischer–Tropsch method. Chem. Geol. 349–350, 27–35.

Zhang, P., Liu, G., Cai, C., Li, M., Chen, R., Gao, P., Xu, C., Wan, W., Zhang, Y., Jiang, M., 2019. Alteration of solid bitumen by hydrothermal heating and thermochemical sulfate reduction in the Ediacaran and Cambrian dolomite reservoirs in the Central Sichuan Basin, SW China. Precambrian Res. 321, 277–302.

Zhao, Y., Truhlar, D.G., 2008. The M06 suite of density functionals for main group thermochemistry, thermochemical kinetics, noncovalent interactions, excited states, and transition elements: two new functionals and systematic testing of four M06-class functionals and 12 other functionals. Theoretical Chemistry Accounts 120, 215–241.

Zhu, G., Zhang, S., Su, J., Huang, H., Yang, H., Gu, L., Zhang, B., Zhu, Y., 2012. The occurrence of ultra-deep heavy oils in the Tabei Uplift of the Tarim Basin, NW China. Organic. Geochemistry 52, 88–102.

Zhu, G., Zhang, Y., Zhang, Z., Li, T., He, N., Grice, K., Neng, Y., Greenwood, P., 2018. High abundance of alkylated diamondoids, thiadiamondoids and thioaromatics in recently discovered sulfur-rich LS2 condensate in the Tarim Basin. Org. Geochem. 123, 136–143.

Zhu, G., Zhang, Y., Zhou, X., Zhang, Z., Du, D., Shi, S., Li, T., Chen, W., Han, J., 2019a. TSR, deep oil cracking and exploration potential in the Hetianhe gas field, Tarim Basin, China. Fuel 236, 1078–1092.

Zhu, Z., Li, M., Tang, Y., Qi, L., Leng, J., Liu, X., Xiao, H., 2019b. Identification of phenyldibenzothiophenes in coals and the effects of thermal maturity on their distributions based on geochemical data and theoretical calculations. Org. Geochem. 138, 103910.